

ORIGINAL ARTICLE

Fluid Flow Analysis Through a Variable Diameter Infra-Red Suppression Device

Avik Bhattacharya^{1,2*} and A. Madhusudan Achari¹¹Mechanical Engineering Department, Institute of Technology, Nirma University, Ahmedabad, Gujarat, India²ITER-India, Institute for Plasma Research, Gandhinagar, Gujarat-382428, India

ABSTRACT – An infra-red suppression device (IRS) is used for suppression of heat signatures from the exhaust of the ships or aero planes, thus facilitating in the stealth operation. In the past, studies have been performed on multiple funnel type, lobed shaped as well as straight funnel type IRS device. In the present study an attempt has been made to suggest a variable diameter IRS device which works on the principle of mass suction due to drop in pressure resulting from the high velocity exhaust fluid. The multiple funnel type IRS device has been modified into an inverted fulcrum like device with holes present on the periphery of device for suction of fluid. Two types of computational studies have been performed. In the first study, the suction is occurring through the bottom as well as the holes on the periphery of funnel wall. In the second study, suction is occurring only through the holes on the funnel wall and bottom of funnel has been kept closed. The mass suction ratio has been calculated for varying Reynolds number of $3000 \leq R \leq 7000$. The effect on suction due to position of holes, number of holes and distance of the holes from the nozzle and effect of bidirectional flow has been computed. It is found that the mass suction ratio is more when suction is occurring through the bottom of the funnel along with the holes on the funnel wall periphery.

ARTICLE HISTORYRevised: 12th Oct 2019Accepted: 8th Feb 2020**KEYWORDS***Infra-red, Suppression, Variable diameter.***NOMENCLATURE**

D_{cd}	diameter of computation domain
D_{ft}	diameter of funnel top
D_{fb}	diameter of funnel bottom
D_{nz}	diameter of nozzle bottom
H_{cd}	height of computation domain
H_f	height of the funnel.
L_p	length of protrusion
T_{nz}	temperature at nozzle exit
T_{sur}	surrounding temperature of ambient air
S_m	sum of body forces
U	velocity magnitude
C_μ	k- ϵ turbulence model constant
m_{suc}	mass suction
m_{in}	inlet mass
μ_{eff}	effective viscosity accounting to turbulence
μ	dynamic viscosity
μ_t	turbulent viscosity
ρ	density
p'	modified pressure.
k	turbulence kinetic energy
ϵ	turbulence eddy dissipation rate

INTRODUCTION

Infrared suppression devices are being used for the suppression of the heat signatures coming out of the exhaust of the aeroplanes and naval ships. This is helpful in a stealth operation. It is quite useful during wars where avoiding detection by stealth surveillance of the enemy is important. The infra-red suppression device is kept near the nozzle exit. Exhaust gases of combustion exits from the nozzle at a high velocity. These high-velocity gases create a low pressure region near the holes, which facilitates for the air to enter through the holes. The air entering through the holes is at atmospheric temperature. The mixing of this low-temperature air with the high temperature exhaust gases results in the overall decrease

in the temperature of the exhaust gases. By simple law of thermodynamics, more the mass of cold air, more will be the reduction in temperature. Thus, ingress of as much mass as possible is the prime objective of any IRS device.

A lot of study and investigations have been done in the past on IRS devices. The entrainment rate by a turbulent air jet is investigated by Ricou and Spalding [1] by varying nozzle exit Reynolds number (based on nozzle diameter) in the range of 2000-80000. The entrainment rate was reported to decrease with Reynolds number when it is varied in a lower range. However, they concluded that the local entrainment by the jet is strongly dependent on the axial distance.

Research has been carried out on aero vehicles like helicopters in order to explore various innovative ways to suppress infrared signals emitted from the exhaust. The effects of mixer configuration on the aerodynamic performances and infrared radiation intensity of the exhaust system of the turbofan engine was studied by Shan and Zhang [2]. The effect of the exhaust temperature on an infrared helicopter signature has been studied numerically by Chen-Xiong et al. [3]. They demonstrated that the radiation intensity from a helicopter is influenced by the exhaust gas temperature for a particular value of skin emissivity. However, for a specific exhaust gas temperature, a surface with low skin emissivity would be beneficial to suppress the radiation. So skin emissivity is an important factor which affects the infrared radiation significantly. Wang and Li [4] have studied the mixing effectiveness of a lobe-ejector combined with a double-wall diffuser. The effects of area ratio of the primary flow and the secondary flow, as well as the speed of the primary flow on the ejected flow-rate ratio, the ejected flow-rate ratio from the gap of the double walls and the distribution of the mixing velocity have been studied and reported.

The DRESS Ball IR signature suppression (IRSS) system for marine gas turbines was developed for Canadian Navy ships and is based on a concept originating from the Defense Research Establishment Suffield (DRES). Brik and Vandam [5] carried out a parametric study for a 1/4 scale DRESS Ball IRSS device, and compared the results with a full-scale sea model. The DRESS Ball IRSS device was installed on the exhaust of the GE LM2500 gas turbine. They investigated the parameters, such as metal surface temperature, back pressure, plume temperature, and static pressure distributions. Thompson et al. [6] discussed possible methods, such as the use of special paints to conceal the hot spots and installation of IRSS devices at the exhaust of the gas turbine to reduce the plume temperature.

A study has been carried out by Tyagi and Subbarao [7] for the use of water mist for plume infra-red suppression. In this study, they have considered water mist as a possible source of the Infra-red signature suppression. They have concluded that the turbulence created by the mixing of water mist with the hot plume gases has resulted in an effective decrease in the temperature. Various studies have been carried out in which the effect on heat transfer due to the protrusions on a flat surface and the effect of different shapes on protrusions. Casanova and Ortega [8] studied the heat transfer between impinging jets and non-uniform heated plates and analysed if surface variations along the plates can improve the heat transfer phenomenon. Barik et al. [9] studied the heat transfer performances of a nanofluid jet impinged normal to a protruded surface. They concluded that heat transfer increased with the increase in no. of protrusion on the surface. Similar studies for the effect of surface protrusions on a surface for heat transfer has been done by Mukherjee et al. [10] and Barik et al. [11].

Studies related to the IRS devices for the naval ships or ships of the merchant navy, to the best of our knowledge, have been less compared to that done for aero vehicles. Recent studies include that by Mishra and Dash [12], who studied the air entrainment into a louvred funnel using a high-speed turbulent jet and Sahu and Mishra [13], who gave an understanding the flow of air through the louvres in a cylindrical pipe. Mishra and Dash reported that the mass suction ratio increases with the louvred opening area; however, their dependency on the louvre numbers was not much. The louvres must be placed in the lower region of the funnel to create a high suction of air into the louvred funnel. Their study provided lots of valuable information on mass ingress into a single diameter louvred funnel. The effect of the injection hole diameter on the operating condition of the fuel injection system of the hydrogen engine was studied by Kamil and Rehman [14]. They have used the concept of the equivalent diameter of the holes for achieving the effect of the hole diameter on the injection system. The in-cylinder flow characteristics inside an internal combustion engine was studied by Hamada et al. [15]. They investigated the effect of the engine speed and equivalence ratio on the flow-field characteristics and volumetric efficiency, in the motoring condition.

Barik et al. [16] have used a scaled-down model as compared to a full-scale model used by Mishra and Dash to study the mass ingress through a straight louvred funnel. The results obtained by Barik et al. conform with that obtained by Mishra and Dash. However, Mishra and Dash [12] have not studied the effect of hot fluid on the mass ingress. Barik et al [16-18] carried out a study with hot as well as with cold nozzle fluid to investigate the mass entrainment ratio by a laboratory-scale IRS device as a function of different pertinent input parameters. A new empirical co-relation for the entrainment ratio was also provided in their work by Barik et al. [19]. It can be seen from above that studies have been performed using a louvred funnel in which it was concluded that the placement of the louvres near the nozzle entry point provides a higher suction of air. However, if the mass entrainment is compared with that of traditional IRS device (figure.1), as reported by Barik et al. [17], then it can be concluded that mass entrainment is lower in case of louvred funnel. It can also be seen that suction remains appreciable even if the annular space is placed far away from the nozzle entry.

In this paper, an attempt has been made to suggest a variable diameter louvred IRS device in which the annular spaces L1, L2 and L3 shown in Figure.1(a) are replaced with louvres of equal total area and suction has been computed through simulation. The effect of hot fluid on the suction rate has already been reported by Barik et al. [16, 17]. A multiple funnel type IRS device in Figure 1(a) has been modified into a variable diameter funnel with holes on the periphery, as shown in Figure 1(b), with D_f/D_{nz} as 6.4, 8.8, 11.2 and 14.4 in Figure 1(a) while the corresponding H_f/D_{nz} are 24, 20, 16, 12. The study has been performed in two parts. In the first part of the study, the annular space at the L1, L2 and L3 in Figure 1(a)

level has been replaced with multiple holes having the same total area as that of the annular space at each level. The arrow near the holes in Figure 1(b) represents the direction of air entry. The bottom of the funnel has been kept open for mass suction. For the second part of the study, the bottom of the funnel has been closed and replaced with holes of equal area. For both the above cases, variation in the mass suction ratio has been studied for different geometrical and flow parameters. The dimension of the nozzle, the bottom and top diameters of the variable diameter funnel, the height of the holes has been kept in accordance with the study performed by Barik et al. [17].

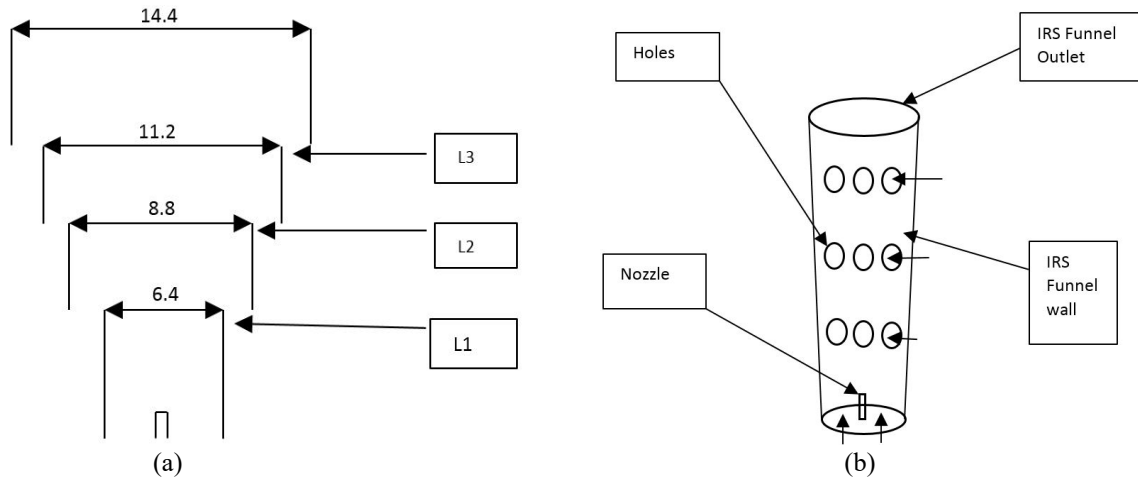


Figure 1. (a) Traditional IRS and (b) proposed IRS device.

MATHEMATICAL FORMULATION

The k-ε model has been used for solving the problem. k is the turbulent kinetic energy and is defined as the variance of the fluctuations in velocity. For the k-ε model, the continuity equation [20] is given in Eq. (1):

$$\frac{\partial \rho}{\partial t} + \frac{\partial(\rho U_j)}{\partial x_j} = 0 \tag{1}$$

The momentum [20] is given in Eq. (2), where, $\mu_{eff} = \mu + \mu_t$, the value of “ μ_t ” can be derived from Eq. (3). The k-ε model assumes that the turbulence viscosity is linked to the turbulence kinetic energy and dissipation as shown in Eq. (3). The mass suction is calculated as per formula in Eq. (4):

$$\frac{\partial \rho U_i}{\partial t} + \frac{\partial}{\partial x_j} (\rho U_i U_j) = - \frac{\partial p'}{\partial x_i} + \frac{\partial}{\partial x_j} \left[\mu_{eff} \left(\frac{\partial U_i}{\partial x_j} + \frac{\partial U_j}{\partial x_i} \right) \right] + S_M \tag{2}$$

$$\mu_t = C_\mu \rho \frac{k^2}{\epsilon} \tag{3}$$

$$m_{suc} = (m_{out} - m_{in}) / m_{in} \tag{4}$$

COMPUTATIONAL MODEL

Conservation equation of mass/continuity equation, momentum equation, Transport equations for turbulent kinetic energy (k) and transport equation for dissipation rate of turbulent kinetic energy (ε) has been integrated over a control volume using finite volume technique. The volume has been discretised using tetrahedral elements while the solution has been done using available code for fluid flow [20]. The Standard k-ε model with scalable wall function has been used for solution of the conservation equation. Log-law wall function has been used for capturing the effect of near-wall elements as reported in the work of Chen-Zong P. et al. [3] and Barik et al. [19]. A comparison study among the standard, realizable and RNG k-model has been reported by Barik et al. [17], and the standard k-ε model has been concluded to be preferable. The study has been done to compute the mass suction ratio as shown in Eq. (4). The model was first solved using first-order upwind scheme and convergence was achieved. For better accuracy second-order upwind scheme has been used. A mesh convergence study (Figure 2) was performed to ensure that results are independent of the grid size. It was found that above ≈ 280 000 elements, the mass suction ratio was showing a minimal variation in each (within 2%). Higher accuracy could have been achieved by refining the mesh, but this would have added to the computational cost and time. Also, for the standard k-model to work, the Y+ value should be above 30. Refining the mesh near the wall and the holes decreased the Y+ value below 30. The model has been meshed using 3,00,000 elements, with refined mesh at the holes, funnel wall near holes, the bottom face of funnel (for the first part of the study only) and the nozzle inlet.

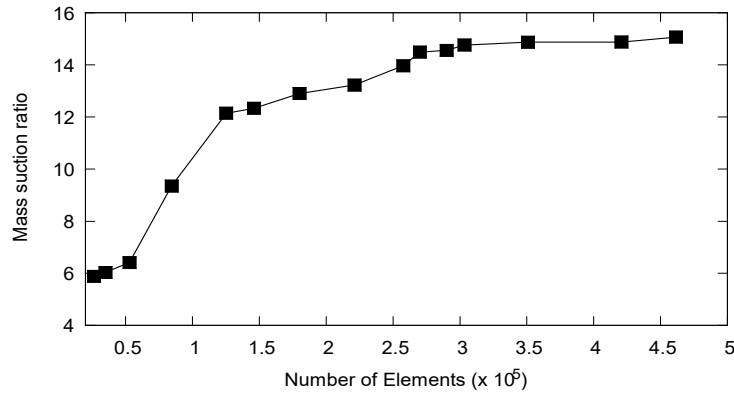


Figure 2. Grid independence plot.

The details of boundary conditions can be found in Figure 3 and Figure 4. The computational domain has been given a pressure outlet boundary condition (denoted by red color in Figure 4(a) on all the faces. The nozzle entry has been given as velocity inlet condition as denoted by blue colour in Figure 4(b). The nozzle and the funnel walls have been given a no-slip and no-shear boundary condition as denoted by white colour in Figure 4(b). The louvres are represented in orange colour. The IRS funnel outlet has been given a pressure outlet condition. The turbulent intensity has been set at 2% at all velocity outlet conditions, and for all pressure outlet condition, the turbulent intensity has been maintained at 5%. Air has been considered as fluid for this study and density has been kept as a function of temperature. The diameter of the nozzle is 0.0125 m. The bottom diameter of the funnel is taken as per ratio D_{fb}/D_{nz} , which is 6.4. The top diameter of the funnel is the ratio D_{ft}/D_{nz} , which is 14.4. The holes have been kept at L1, L2, and L3 location (Figure 1) for the first study and the bottom of the funnel has been kept open. In the second study, the bottom opening has been replaced by another row of holes of the same total area.

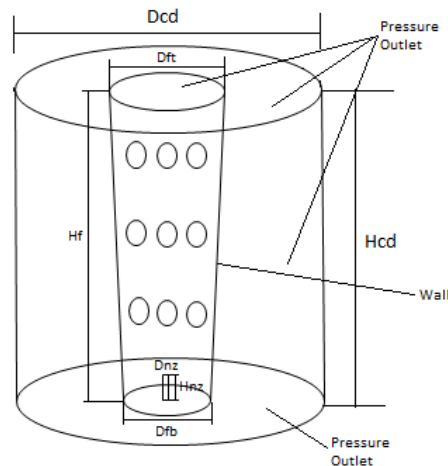


Figure 3. Boundary conditions.

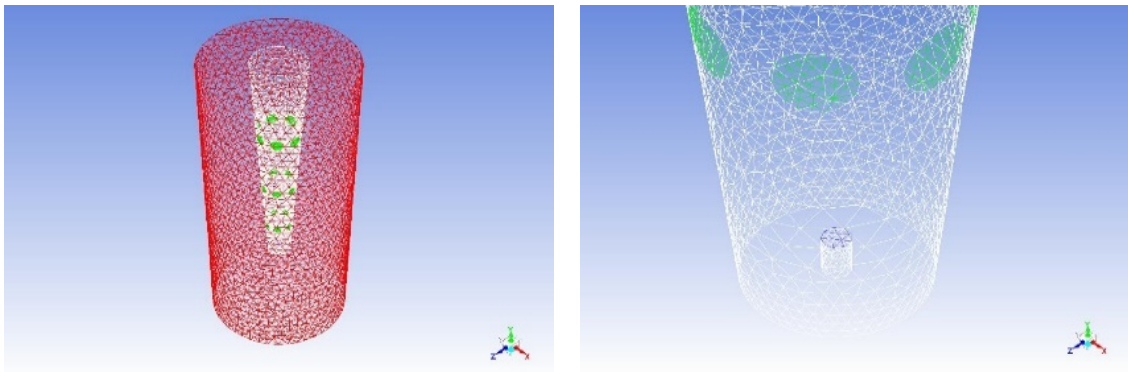


Figure 4. Boundary conditions applied.

VALIDATION OF EXPERIMENTAL RESULTS IN CFD

Before starting with the actual study on the proposed IRS devices, the experimental results by Barik et al. [16, 17] was validated with the results generated in Ansys code for fluid flow [20] for gaining confidence in the software operation as well in the simulation procedure. The validation has been done for two separate studies by Barik et al. [16], [17].

Study of Mass Entrainment in a Straight Louvred Funnel

Barik et al. [16], studied the entrainment ratio in a straight louvred funnel. The model for the study was generated in Ansys design modeller. The effect on the entrainment ratio due to various parameters was computed and reported.

Reynold's number

The entrainment ratio has been calculated for varying the Reynolds number. The variation of entrainment ratio with the change in Reynolds number has been presented in Figure 5 with a close conformation in simulation and experimental results. It can be noted that with the increase in Reynolds number, the suction of cold air increases. However, the effect on the ratio is negligible.

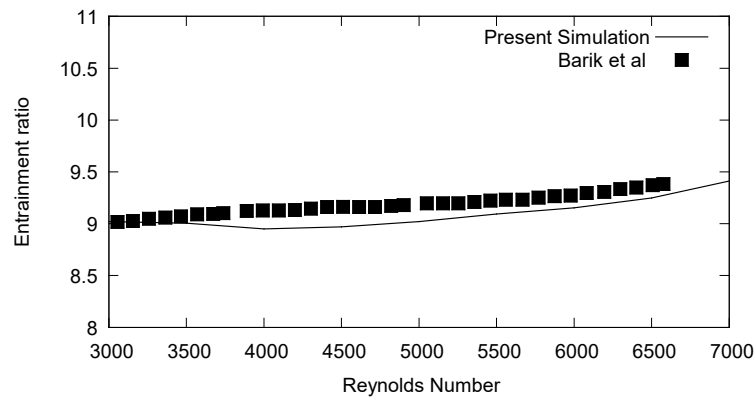


Figure 5. Variation of entrainment ratio with Reynolds number.

Nozzle protrusion length

The entrainment ratio was calculated by varying the protrusion length of the nozzle. Protruding length is the length by which the nozzle is inserted inside the funnel from the bottom. In Figure 6 the x-axis represents the nozzle protrusion length as a ratio of nozzle diameter. It can be seen that up to nozzle protrusion ratio of 5, the entrainment ratio increases significantly. From 6 to 8, there is a slight decrease in the slope, which indicates that the ratio variation is decreasing while above 8, the ratio becomes constant.

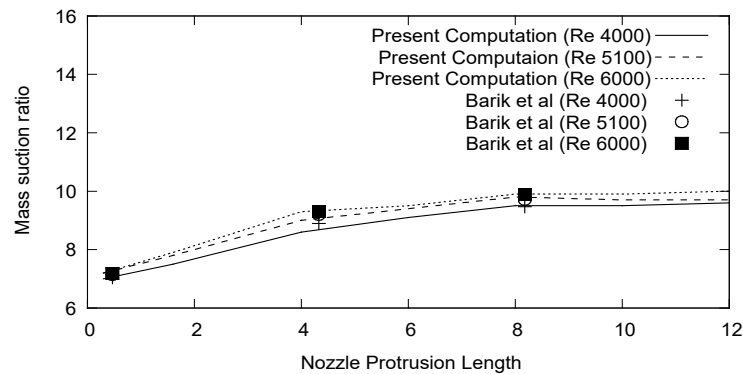


Figure 6. Effect of nozzle protrusion length on entrainment ratio.

Total louvred area for different temperature ratios

The variation in the entrainment ratio with the change in the louvre opening area was computed. As the area was increased, the entrainment was increasing. The entrainment was highest when all the louvres were open for entrainment. So larger opening area result in more entrainment. In Figure 7, the x-axis shows the ratio of louvre opening area to that of the area of the nozzle.

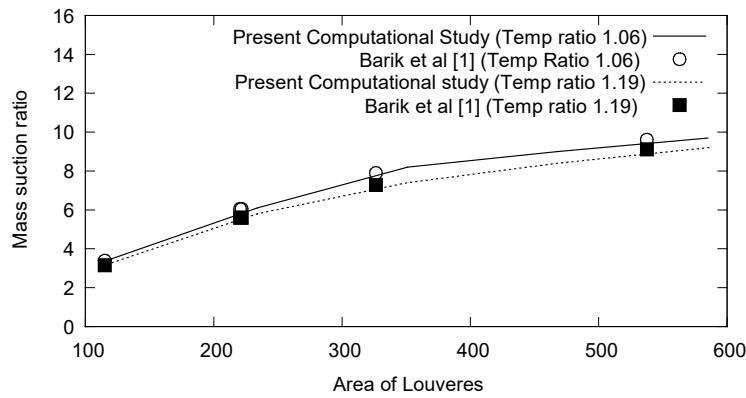


Figure 7. Effect of louvre opening area on mass suction.

Study of Mass Entrainment in Multiple Funnel Type IRS Device

Barik et al. [17] studied the entrainment ratio in an IRS device. The effect on the entrainment ratio due to various parameters are computed and reported below.

Funnel overlap height

The funnel overlap height has been varied and the effect on the entrainment ratio has been calculated and shown in Figure 9. In a zero overlap condition, when a funnel is placed above other, the top of one funnel is in the same plane as the bottom of the funnel above it. In Figure 8, for positive overlap condition, the bottom funnel goes inside the top funnel. As for the negative overlap condition, there is a gap between the top of the bottom funnel and the bottom of next funnel. From Figure 9, it is evident that the zero overlap condition yields the maximum suction. The mass suction in case of positive overlap condition is better as compared to the negative overlap condition.

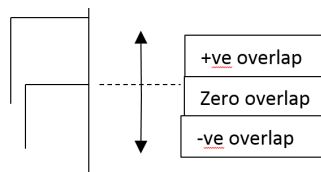


Figure 8. Positive, negative and zero overlap condition.

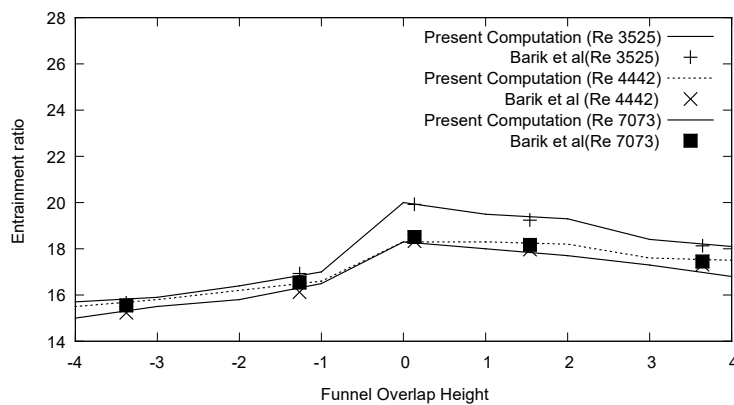


Figure 9. Variation of entrainment ratio with funnel overlap height.

Temperature ratio(T_{nz}/T_{surr})

The effect on nozzle fluid inlet temperature on the entrainment of fluid has been studied. As the inlet fluid temperature increases so do the mass of air being entrained. However, from Figure 10 the effect of increasing Reynolds number can be seen up to Reynolds number 6500 in the case of temperature ratio of 1.06 and 1.18. After that, the entrainment ratio remains almost constant. In case of temperature ratio of 1.01, the entrainment ratio remains the same for all Reynolds number.

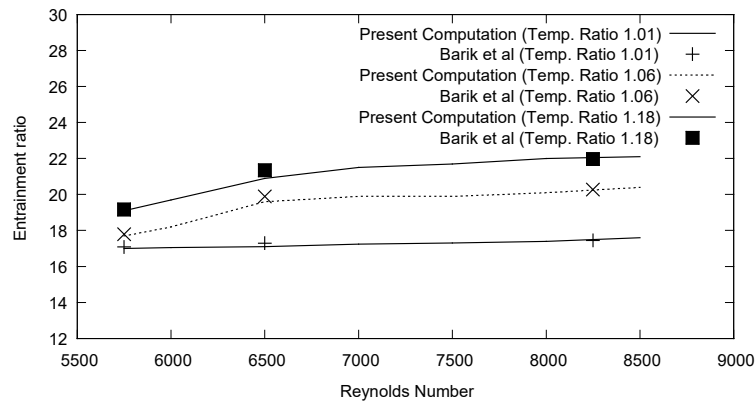


Figure 10. Variation of entrainment ratio with Reynolds number for different temperature ratios.

Nozzle protrusion length

The effect of nozzle protrusion inside the nozzle has been calculated and shown in Figure 11. The optimum nozzle height has also been calculated. The x-axis of the graph represents the Nozzle protrusion length ratio (L_p/D_{nz}) with the diameter of the nozzle. Up to nozzle protrusion length ratio of 2, the entrainment keeps on increasing, but after that, the entrainment ratio keeps on decreasing and becomes steady after nozzle protrusion length of 4. So the optimal nozzle protrusion length for maximum air suction was found to be 2.

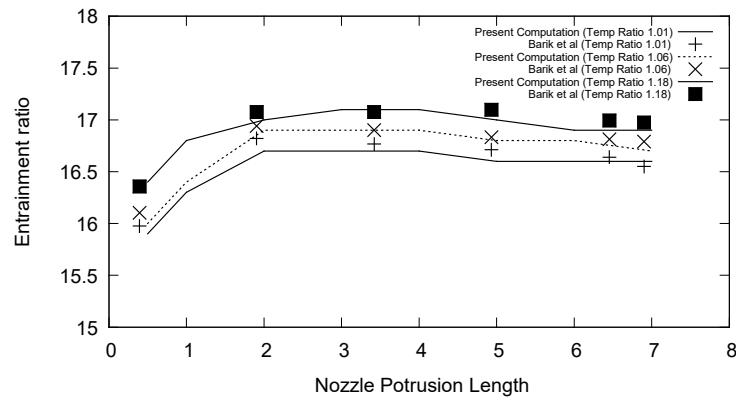


Figure 11. Effect of nozzle protrusion length on entrainment ratio.

RESULTS AND DISCUSSION

IRS funnel bottom open

The annular space at the location of funnel overlap has been replaced with holes of the same total area as that of the annular space. However, the annular space between the nozzle and the funnel has not been replaced with holes and has been kept as it is. The mass suction ratio for various conditions has been computed and reported. The temperature has been kept at 304 K because earlier studies have already reported an increase in entrainment ratio with an increase in the inlet fluid temperature. The same was done as a part of the validation of previous results. In Figure 12, streamline plot for velocity at Reynolds number 3000 has been shown to give an impression of the flow occurring during mass suction.

Reynold's number

The Reynolds number (Re) of the inlet jet was varied in the range of $3000 \leq R \leq 7000$, and the variation in the mass suction ratio was observed. The graph in Figure 13 shows the Reynolds number in increasing order in the x-axis and the mass suction ratio in the increasing order in the y-axis. It can be seen from the graph that the mass suction ratio varies linearly with the increase in Reynolds number. However, a downward trend is observed in the mass suction ratio, when we keep on increasing the velocity of the inlet fluid. The variation is approximately 2% which is negligible. This may be due to the fact that as we keep on increasing the velocity for fluid flow through the same area, losses increase which results in lower mass suction ratio.

Number of holes

The total number of holes in each row was varied keeping the total area of all the holes same as that of the annular space. With the increase in the number of holes, the size of individual holes decreased. The variation in the mass suction has been shown below in Figure 14. It has been observed that up to two holes, the mass suction was low. Up to 4 holes, the mass suction ratio increases with the number of holes. However, when we increase the holes beyond that, the mass

suction ratio remains more or less constant. This matches with that reported by Mishra and Das in their paper that mass suction ratio is independent of the no. of holes as long as the total area of suction remains the same. This is in line with the continuity equation as the total area remains the same and the entrainment at each level for a particular Reynolds number is constant. The graph below shows the variation of the suction ratio with the number of holes. The x-axis indicates the number of holes and the Y-axis shows the Mass suction ratio. The variation for different Reynolds number is shown starting from Reynolds number 3000 up to 7000.

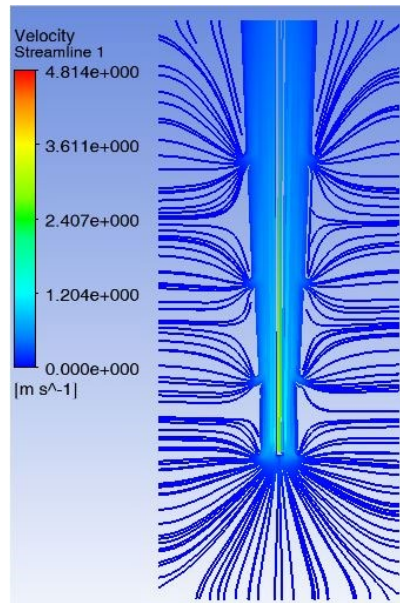


Figure 12. Velocity streamline for Reynolds number of 3000.

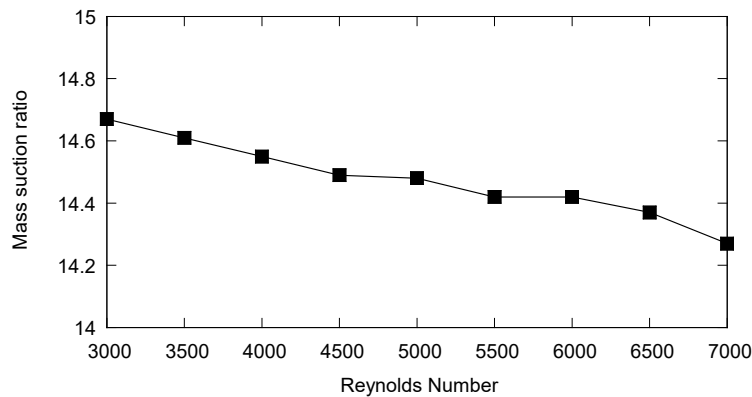


Figure 13. Variation of mass suction ratio with changing Reynold’s number.

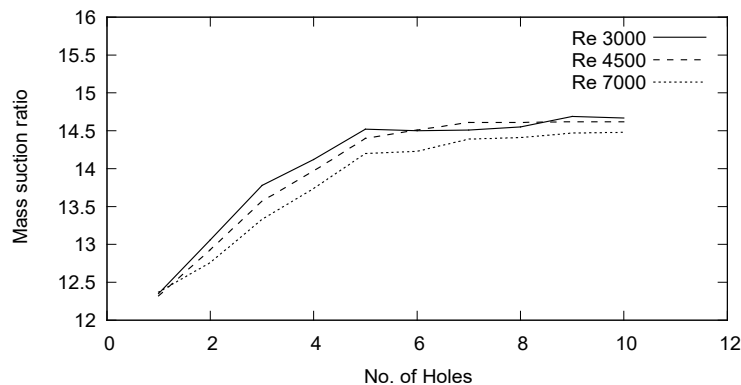


Figure 14. Variation of mass suction ratio with the number of holes.

Change in distance of the holes from then nozzle entry point

The holes were removed from their original location and, as reported by Barik et al. [16] and Mishra and Das [12], were kept near the nozzle entry point as shown in Figure 15. The distance between each row of the holes was maintained at 0.04 m. The mass suction ratio was then computed by gradually moving the holes away from the nozzle exit. Overall variation in the mass suction ratio was computed. Figure 16 shows the distance of the holes from the nozzle in the x-axis and the mass suction ratio in the y-axis. It can be seen from the graph in Figure 16, that with an increase in distance from the nozzle entry point, initially there is an increase in mass suction up to 0.2 m from the nozzle entry and after there is a continuous decrease in the mass suction through the holes. But the overall reduction in mass suction is quite less. This is because, in this case, the mass suction is not dependent on holes only. There is continuous mass suction from the bottom of the funnel.

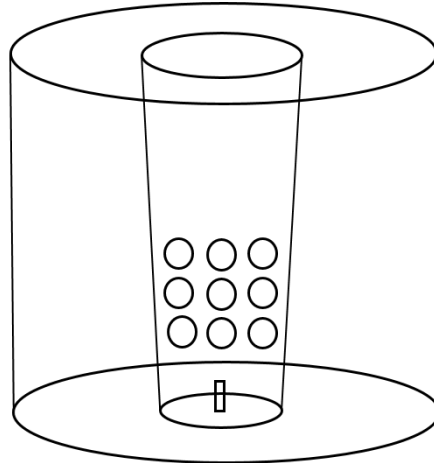


Figure 15. Holes location from nozzle entry.

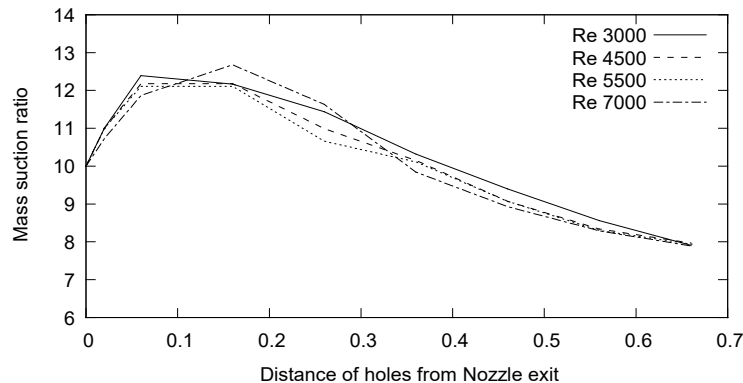


Figure 16. Variation of mass suction ratio due distance of holes from nozzle exit.

Symmetrical and asymmetrical placement of the holes in the IRS funnel

The holes in each row are placed symmetrically with respect to each other i.e. hole in each row is directly above the holes in the previous row. It can be seen, the holes have been asymmetrically placed as shown in Figure 17 and 18 where the vertical axis of the hole in a particular row is having an offset with the axis of hole in the row below.

In the graph of Figure 19, it can be seen that in case of a funnel in which bottom is open where air is entering through the bottom of the funnel, the mass ingress through the symmetrical placement of holes is higher than that obtained in the asymmetrical placement of the holes. This might be because the symmetrical placement of holes offers less restriction to the flow of air occurring from the open bottom of the funnel as compared to the asymmetrical placement.

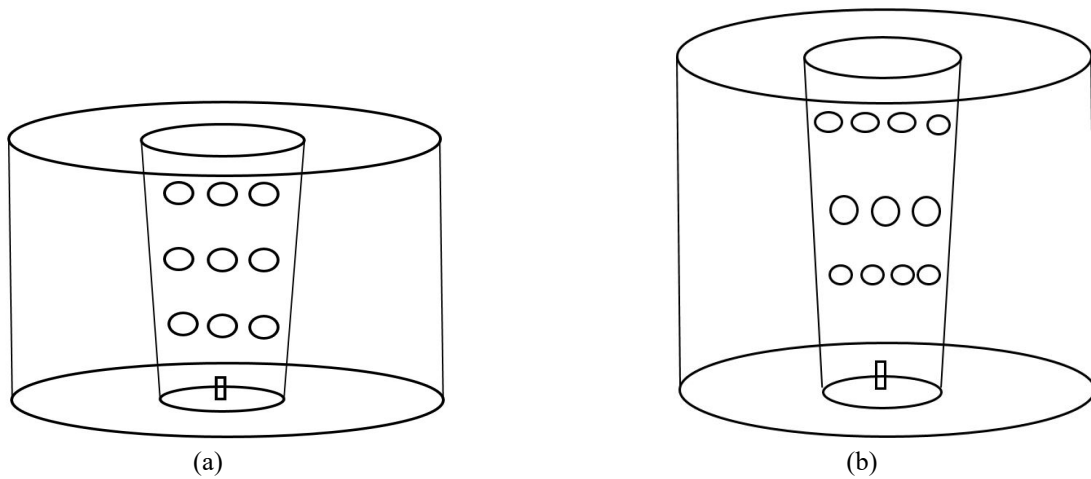


Figure 17. (a) Symmetrical and (b) asymmetrical placement of holes.

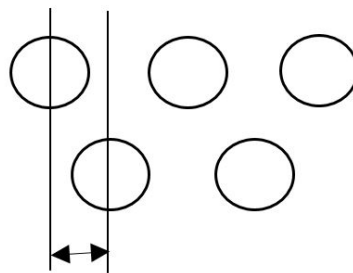


Figure 18. Offset in asymmetrical placement of holes.

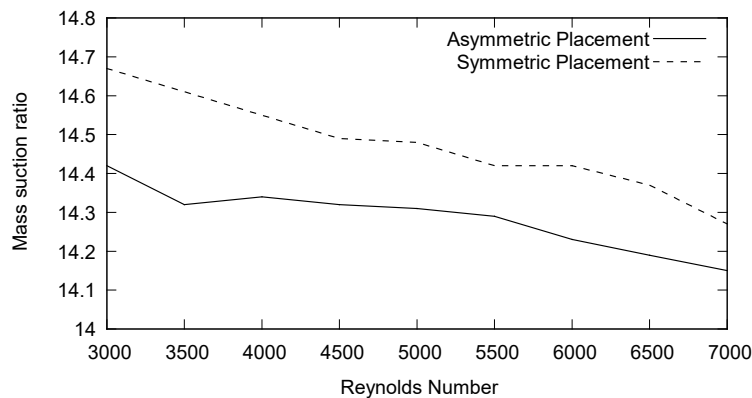


Figure 19. Change in mass suction due to the placement of holes.

Nozzle protrusion length

The effect of the nozzle protrusion in on the mass suction through the louvres has been computed. If the nozzle entry is kept nearer to the louvre opening area, then the mass suction increases. However, as the nozzle entry point is kept away from the holes opening area, the mass suction shows a slight dip. It is however seen that the nozzle opening should be kept closer to the bottom opening only as this gives the maximum mass suction ratio through the louvres. If we keep the nozzle opening near the first row of the holes, the mass suction is lower. This can be attributed to the fact that when the mass suction through the bottom opening is maximised, it facilitates the mass suction through the other row of holes above it. In the graph of Figure 20, it can be seen that when the nozzle entry is kept near the bottom opening the mass suction ratio is high. As the nozzle entry is moved away from the bottom opening; i.e. as the nozzle protrusion height increase, the mass suction decrease and after 0.03 m the variation is negligible

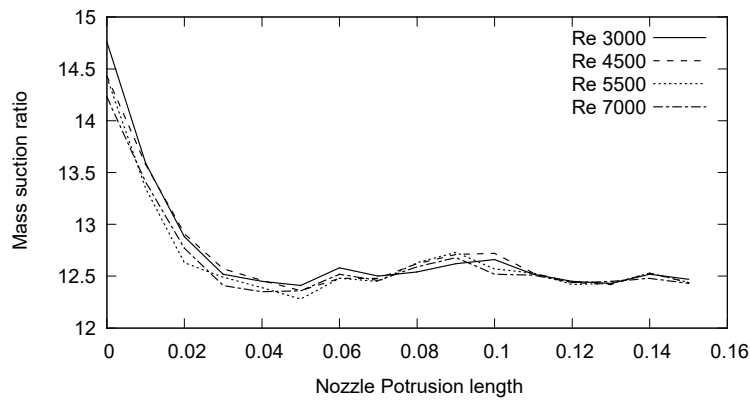


Figure 20. Change in mass suction with nozzle protrusion length.

Nozzle distance from the funnel bottom

In the previous case, the nozzle distance from the bottom of the funnel was varied, and computation study has been done. As the nozzle is moved nearer to the funnel bottom the mass suction ratio is increasing. However, the variation is not completely linear as can be seen from the graph in Figure 21. This is due to the fact that as we move nearer to the nozzle, the mass suction increases and so does the frictional effect of the flow at the holes. This slightly restricts the flow. The computation has been done for increasing Reynolds number to see the effect of Reynolds number on the mass suction ratio. There is a slight decrease in the mass suction ratio with the increase in Reynolds number, however, the change is not significant. This might be due to the friction affecting the flow when a high-velocity fluid enters through the enclosed area. If we keep the area same and increase the velocity, frictional effect increases and restricts the flow.

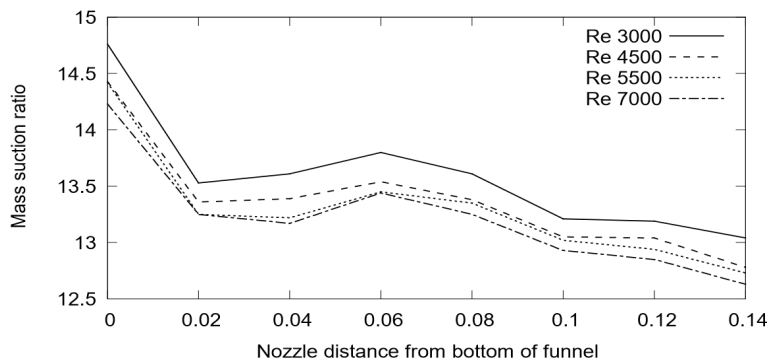


Figure 21. Change in mass suction due to change in distance of the nozzle.

Contribution percentage of each row of holes and the bottom opening in the total mass suction

In this study, the amount contributed to the mass suction ratio by each row of holes is calculated and reported. It can be seen from the results that as we move away from the nozzle outlet, the mass suction occurring as compared to the previous row of holes' decreases. This is because as we moved away from the high-velocity region, the low pressure created near the holes in each row that facilitates the suction decreases. As a result, the mass sucked through those particular row of holes is decreased. From the graph in Figure 22, 1 represents the open bottom, and 2, 3 and 4 represent the consecutive row of holes. The holes are represented in the x-axis. The y-axis represents the percentage contribution. The percentage contribution of each row of holes is shown. The first row of holes shows the maximum suction of mass, and it subsequently decreases as we move above towards the funnel exit.

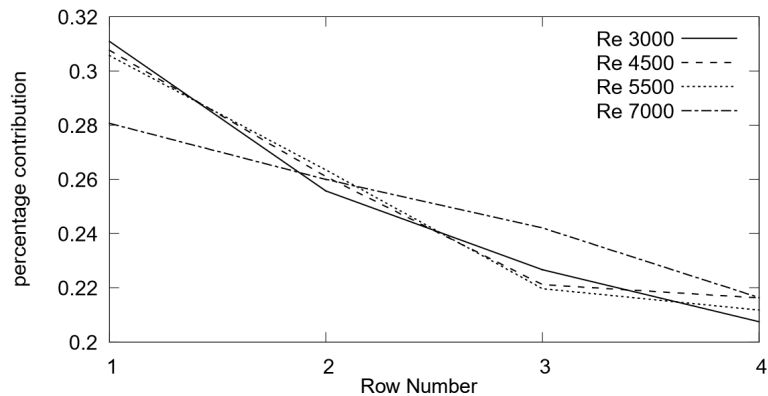


Figure 22. Percentage contribution of holes in mass suction.

IRS funnel with closed bottom and replaced by holes of the same total area

In this case the bottom face of the funnel has been considered as closed face and wall condition has been applied. The face has been replaced by a row of holes which has the same total area as that of the bottom face as shown in Figure 23. This is done to see the effect on the mass suction inside the funnel.

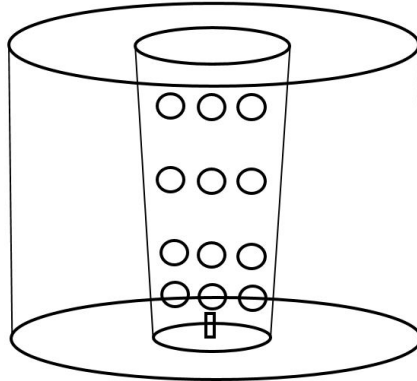


Figure 23. The bottom face of the funnel is closed and replaced with holes of equal total area.

Reynold's number

The Reynolds number (R) of the inlet jet was varied in the range of $3000 \leq R \leq 7000$, and the variation in the mass suction ratio was observed. It can be seen from the graph in Figure 24 that the mass suction ratio varies linearly with the increase in Reynolds number. However, there is no significant change in the mass suction ratio.

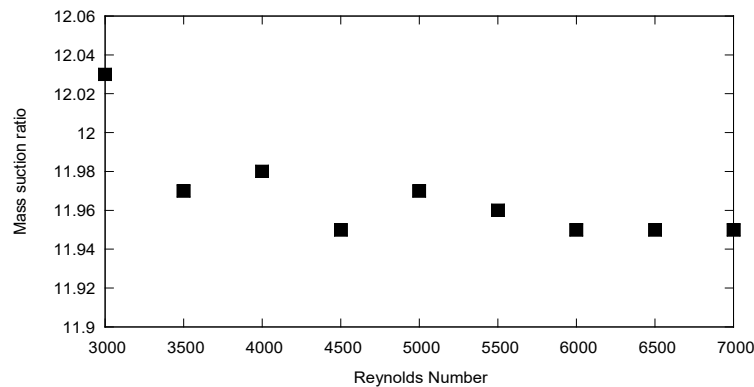


Figure 24. Variation of mass suction with Reynold's number.

Change in distance of the holes from the nozzle

The arrangement of the holes in this case has been changed. The holes have been moved from their original location and have been moved close to the nozzle. The distance between the individual rows of holes has been kept constant at 0.04 m. The whole arrangement then kept at various distance from the nozzle inlet. The mass ingress has been calculated for varying three Reynolds number. It can be seen from the Figure 25, that there is a drop in the mass ingress through the nozzle as the holes move away from the nozzle inlet. So it is advisable to keep the holes near the nozzle inlet to get the maximum mass ingress through the nozzle.

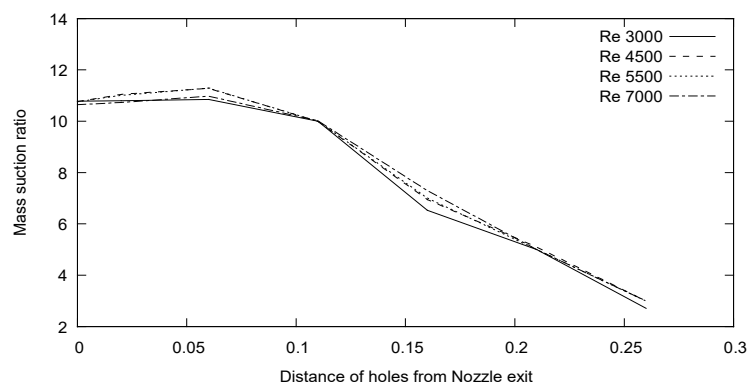


Figure 25. Change in mass suction with change in hole distance from nozzle exit.

Number of holes

The total number of holes in each row was varied, keeping similar to what was done in the previous case. The variation in the mass suction is shown in Figure 26. It is observed that up to two holes, the mass suction was low. From three holes onwards the mass suction ratio increases and remains constant. So the no. of holes does not affect the mass suction ratio once the number of holes is increased beyond 3.

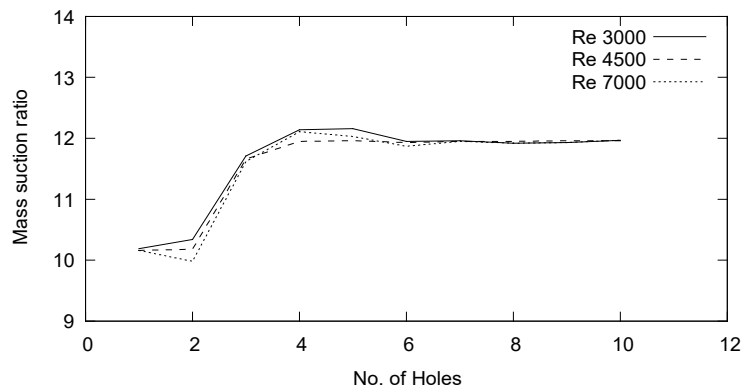


Figure 26. Change in mass suction due to no. of holes.

Placement of holes

As done in the previous study, the holes in adjacent rows are placed asymmetrically to each other (in Figure 17). The vertical axis passing through the centre of the hole in one row is at an angular offset to the vertical axis of the holes in the row just above. The mass suction ratio for this arrangement has been computed for $3000 \leq R \leq 7000$. It can be seen from the graph of Figure 27 that the mass suction ratio for the asymmetric placement of the holes is more as compared to the mass suction ratio in case of symmetric placement of holes. In the previous case, it was opposite. The symmetrical placement of holes was showing more mass suction. However, the bottom was open in the previous case and closed in the current case. So when the mass suction is occurring only through holes, it can be concluded that the symmetric placement of holes yields a lower mass suction ratio. This might be due to the fact that asymmetrical placement of holes might offer less resistance to fluid flow, which resulted in higher mass suction.

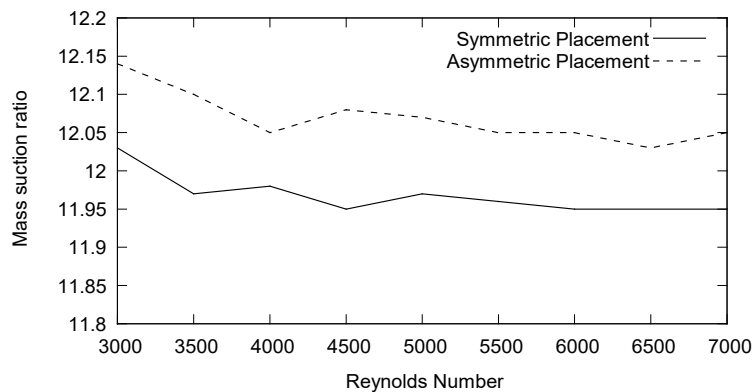


Figure 27. Change in mass suction due to placement of holes.

Nozzle protrusion length

The effect of the nozzle protrusion length on the mass suction through the louvres has been computed. If the nozzle entry is kept nearer to the louvre opening area, then the mass suction increases. However, as the nozzle entry point is kept away from the holes opening area, the mass suction shows a slight dip. It is however seen that the nozzle opening should be kept closer to the bottom row of holes (at 0.04 m) only as this gives the maximum mass suction ratio through the louvres. If we keep the nozzle opening nearer to the second row of the holes, the mass suction is lower as compared to the previous case. This can be attributed to the fact that when the mass suction through the bottom row of holes is maximized, it facilitates the mass suction through the other row of holes above it. The mass suction decreases again when we move away from the nozzle. This produces a zig-zag shaped graph as seen in Figure 28.

Contribution of each row of holes and the bottom opening in the total mass suction

The amount contributed to the mass suction ratio by each row of holes was calculated and reported. It can be seen from the results that as we move away from the nozzle outlet, the mass suction occurring as compared to the previous row of holes decreases. This is because as we move away from the high-velocity region, the low pressure created near the holes in each row that facilitates the suction decreases. As a result, the mass sucked through those particular row of holes is decreased. The graph below shows the result.

In Figure 29, 1 represents the first row of holes and 2, 3 and 4 represent the subsequent row of holes. The holes are described in the x-axis while the y-axis represents the percentage contribution. The percentage contribution of each row of holes is shown. The first row of holes shows the maximum suction of mass, and it subsequently decreases as we move above towards the funnel exit.

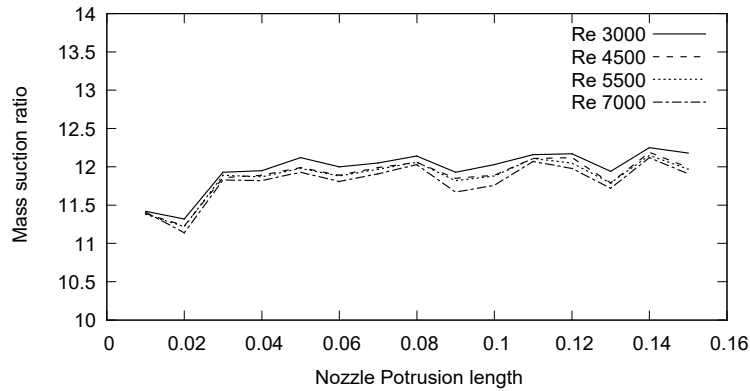


Figure 28. Change in mass suction due to variation in nozzle protrusion length.

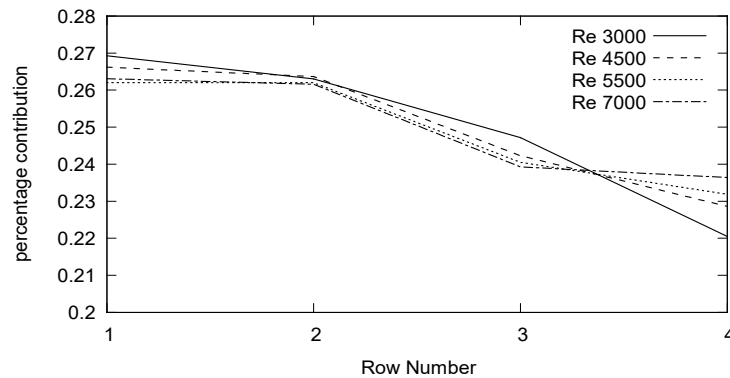


Figure 29. Percentage contribution of holes in mass suction.

Comparison with other IRS devices

In this section, a comparison has been shown in Figure 30 for variation of the mass suction ratio with the Reynolds number amongst a conventional/traditional IRS device [17], a straight louvred funnel type IRS device [16] and the proposed variable diameter funnel type IRS device for normal temperature condition.

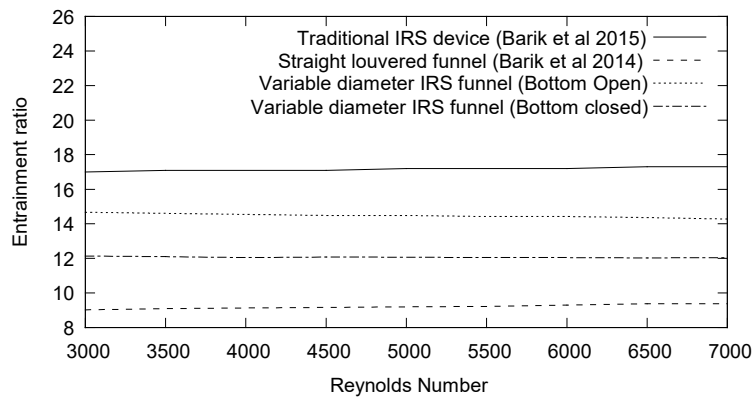


Figure 30. Comparison of mass suction ratio of different IRS devices.

CONCLUSION

In the normal temperature operating condition, the maximum mass suction ratio that is obtained from the bottom open condition is 14.7, and in case of the bottom close condition is 12.1. The mass suction increases by ~ 22%. The mass suction through the holes is independent of their number. The placement of holes has an effect on the mass suction. For bottom open condition symmetrical placement is showing higher mass suction than asymmetrical placement. For bottom asymmetrical is showing higher mass suction than symmetrical placement. For bottom open condition, as all the holes are moved away from nozzle inlet, there is a decrease of 38% in the mass suction ratio. However, for the bottom closed condition, the mass suction decreases by almost 75%. For better mass suction, each row of holes should be at some

distance from the previous row with the bottom row nearer to the nozzle inlet. It can also be concluded that if we replace a continuous annular space with holes of equal total area, there is a decrease in mass entrainment by almost 20%. This can be due to; in the case of annular space the direction of mass suction is same as that of the entry fluid, which provides the least resistance to the flow. Whereas, in the case of the funnel with holes, the direction of flow in case of mass suction is perpendicular to that of the nozzle entry flow. This might cause a slight restriction to flow. The percentage contribution of holes decreases when as we move towards the top holes. However, in the bottom open condition, a significant contribution in mass suction is given by the open bottom. So the open bottom condition is suggested for maximum mass suction. The effect of the nozzle protrusion length on the mass suction was computed. In case of the bottom open funnel, it can be seen that the mass suction is maximum when the nozzle entry is kept nearer to the bottom of the funnel. However, for the funnel with only holes, mass suction is maximum when the nozzle is kept near the bottom row of holes. The distance of the nozzle exit also has an effect on the mass suction occurring through the holes with funnel bottom open condition. As the nozzle reaches nearer to the bottom of the funnel, the mass suction increases. So for maximum mass suction to occur, it is advisable to keep the nozzle opening nearer to the funnel bottom. For optimum mass suction, a bottom open funnel with the first row of holes nearer to the nozzle inlet is suggested and the nozzle inlet should be kept as close to open bottom as possible.

ACKNOWLEDGEMENT

I would like to thank my colleagues in Cryostat group ITER-India for their support during the course of this work. I would also like to thank the Head of the department, Mechanical Engineering, Institute of Technology, Nirma university for providing motivation and support during the course of this work.

REFERENCES

- [1] Ricou FP SD. Measurements of entrainment by axisymmetric turbulent jets. *Journal of Fluid Mechanics* 1987; 25(9): 1216.
- [2] Shan Y, Zhang J zhou. Numerical investigation of flow mixture enhancement and infrared radiation shield by lobed forced mixer. *Applied Thermal Engineering* 2009; 29: 3687–3695.
- [3] Pan CX, Zhang JZ, Shan Y. Effects of exhaust temperature on helicopter infrared signature. *Applied Thermal Engineering* 2013; 51: 529–538.
- [4] Wang SF, Li LG. Investigations of flows in a new infrared suppressor. *Applied Thermal Engineering* 2006; 26: 36–45.
- [5] Birk AM, VanDam D. Infrared signature suppression for marine gas turbines: comparison of sea trial and model test results for the DRES Ball IRSS System. *Journal of Engineering for Gas Turbines and Power* 1994; 116: 75.
- [6] Packard TJ, Cited R, Documents USP, et al.. Infrared signature suppression for marine gas turbines: comparison of sea trial and model test results for the DRES Ball IRSS System. *International Journal of Heat and Mass Transfer* 2013; 113: 33–44.
- [7] Tyagi A, Subbarao PM V. Feasibility studies on use of water mist for plume infrared suppression. *International Journal of Engineering Inventions* 2016; 5: 33–44.
- [8] Ortega-Casanova J, Granados-Ortiz FJ. Numerical simulation of the heat transfer from a heated plate with surface variations to an impinging jet. *International Journal of Heat and Mass Transfer* 2014; 76: 128–143.
- [9] Barik AK, Rout S, Mukherjee A. Numerical investigation of heat transfer enhancement from a protruded surface by cross-flow jet using Al₂O₃–water nanofluid. *International Journal of Heat and Mass Transfer* 2016; 101: 550–561.
- [10] Mukherjee A, Rout S, Barik AK. Heat transfer enhancement from a ribbed surface in presence of a cross flow jet : A numerical investigation. *Journal of Material Science and Mechanical Engineering* 2016; 3: 172–178.
- [11] Barik AK, Mukherjee A, Patro P. Heat transfer enhancement from a small rectangular channel with different surface protrusions by a turbulent cross flow jet. *International Journal of Thermal Sciences* 2015; 98: 32–41.
- [12] Mishra DP, Dash SK. Numerical investigation of air suction through the louvres of a funnel due to high velocity air jet. *Computers & Fluids* 2010; 39: 1597–1608.
- [13] Mishra SRS and D. Numerical investigation of maximum air entrainment into cylindrical louvreed pipe. *International Journal of Automotive and Mechanical Engineering* 2016; 13: 3278–3292.
- [14] Kamil Mohammed RM. Effect of Injection Hole Diameter on Operational. *International Journal of Automotive and Mechanical Engineering* 2015; 11: 2383–2395.
- [15] Hamada Khalaf I, Rahaman MM, Ramasamy D, Noor MM K. Numerical investigation of in-cylinder flow characteristics of hydrogen-fuelled internal combustion engine. *Journal of Mechanical Engineering and Sciences* 2016; 10: 1792–1802.
- [16] Barik AK, Dash SK, Patro P, et al. Experimental and numerical investigation of air entrainment into a louvred funnel. *Applied Ocean Research* 2014; 48: 176–185.
- [17] Barik AK, Dash SK, Guha A. Experimental and numerical investigation of air entrainment into an infrared suppression device. *Applied Thermal Engineering* 2014; 75: 33–44.
- [18] Barik AK, Dash SK, Guha A. Entrainment of air into an infrared suppression (IRS) device using circular and non-circular multiple nozzles. *Computers and Fluids* 2015; 114: 26–38.
- [19] Barik AK, Dash SK, Guha A. New correlation for prediction of air entrainment into an Infrared Suppression (IRS) device. *Applied Ocean Research* 2014; 47: 303–312.
- [20] Ansys R17.2. Ansys user manual.